

# Optics Letters

## Control of diameter and numerical aperture of microlens by a single ultra-short laser pulse

HUA FAN,<sup>1</sup> XIAO-WEN CAO,<sup>2</sup> LEI WANG,<sup>1,6</sup>  ZHEN-ZE LI,<sup>1</sup> QI-DAI CHEN,<sup>1,7</sup> SAULIUS JUODKAZIS,<sup>3,4</sup>   
AND HONG-BO SUN<sup>5</sup> 

<sup>1</sup>State Key Laboratory of Integrated Optoelectronics, College of Electronic Science and Engineering, Jilin University, Changchun 130012, China

<sup>2</sup>Ningbo Institute of Materials Technology and Engineering, CAS, Ningbo 315201, China

<sup>3</sup>Centre for Micro-Photonics, Faculty of Science, Engineering and Technology, Swinburne University of Technology, Hawthorn, VIC 3122, Australia

<sup>4</sup>Melbourne Centre for Nanofabrication, ANFF, 151 Wellington Road, Clayton, VIC 3168, Australia

<sup>5</sup>State Key Laboratory of Precision Measurement Technology and Instruments, Department of Precision Instrument, Tsinghua University, Beijing 100084, China

<sup>6</sup>e-mail: leiwang1987@jlu.edu.cn

<sup>7</sup>e-mail: chenqd@jlu.edu.cn

Received 13 August 2019; revised 16 September 2019; accepted 21 September 2019; posted 27 September 2019 (Doc. ID 375366); published 17 October 2019

**We demonstrate a versatile method for fast and flexible fabrication of either one or an array of microlenses. Multi-foci axial intensity distribution generated by a phase pattern displayed on a spatial light modulator irradiates silica, causing ablation and its internal modification. The following wet etching step defines the diameter  $r$ , while the radius of curvature  $R$  (hence, the focal length  $f$ ) is maintained the same. As a result, the numerical aperture  $NA = r/f$  changes from 0.2 to 0.4 for the same pulse energy (but different number of multi-foci) during ablation. An isotropic wet etching of silica becomes highly anisotropic for the initial stages of etching following the irradiated pattern. Subsequent evolution of the shape is governed by an isotropic silica etch and forms a spherical lens. This method can be extended to other materials and geometries of micro-optical elements.** © 2019 Optical Society of America

<https://doi.org/10.1364/OL.44.005149>

The microlens, a basic micro-optical element, has become important in the development of integrated optics [1,2]. It has a significant potential for many applications: optical communications [3], wavefront detection [4], micro-fluidics [5], and liquid crystal displays [6]. A variety of methods have been proposed to directly fabricate microlens arrays (MLAs), including stamping or embossing [7], photolithography [8], photoresist thermal reflow [9], and inkjet imprinting [10]. However, most of the above are multi-step methods with a high cost or confined to only soft materials, which hinders their further applications in harsh and industrial environments. Moreover, the molds for replication into soft materials have to be made using other methods. In order to fabricate a refractive microlens on fused silica, a maskless method was proposed by combining femtosecond (fs)-laser ablation and wet-etching techniques [11,12]. A uniform and arbitrary arrangement of microlenses

has been realized on a flat or curved surface by the direct-write flexibility of the fs-laser microfabrication [13,14]. Good focusing and imaging results have been demonstrated [15]. Although the method is simple and effective, the etched diameter and depth depend mainly on the first zone ablated by the fs laser, and therefore, it is difficult to control the above parameters. Moreover, the two parameters are linearly correlated with one another, resulting in the fabrication of microlenses with a constant numerical aperture NA irrespective of the etching time [16,17]. In addition, for different microlens dimensions, different laser intensities are required, and it greatly affects the processing efficiency and flexibility of fabricating MLAs with varying focal lengths (curvature radius) for zoom-less monitoring applications.

Herein, we propose a light intensity shaping method for microlenses with well-controlled size and NA by modulating the original one-spot-focus into a multi-spot focus along the optical axis using a spatial light modulator (SLM). The high flexibility of SLM makes it easy to realize complex patterns after the objective just by changing the phase pattern [18–20]. With a post-exposure wet etching, the ablated/modified area on/in silica evolves into a micro-concave lens. Size of the microlens is defined by the number of focal spots without changing the pulse energy of the laser and positions on the sample. The axially structured light generated by the hologram displayed on the SLM allows to use a single pulse defining a different size and NA of the microlens.

The schematic of a fs-laser holographic processing system is shown in Fig. 1(a). A fs-laser beam (514 nm wavelength, pulse duration of 230 fs) is incident on a reflection-type liquid crystal SLM (LCOS-SLM, LETO, HOLOEY photonics AG) with a high fill factor of 93%. The reflected phase-modulated beam is transferred to the entrance pupil of the objective lens (NA = 0.7) by a telescope system to downsize the beam diameter with a magnification factor of 0.75 and increase the light utilization efficiency. Then, the modulated laser beam

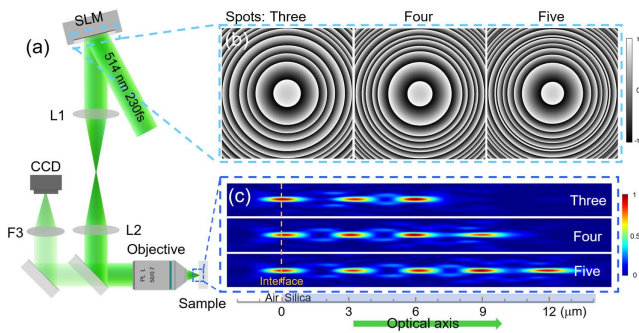


**Fig. 1.** Dynamic femtosecond laser holographic processing system. (a) Schematics of the experimental setup. (b) Multi-focal spots hologram generated by the optimal rotation angle (ORA) method. (c) Multi-focus intensity distribution along optical axis simulated by 3D vectorial diffraction theory; the 0  $\mu\text{m}$  marked in (c) stands for the interface between the air and silica.

is focused on the fused silica sample for ablation/modification. A motorized linear  $xy$  stage with 100 nm resolution and 20 mm  $\times$  20 mm dynamic range is used to move the substrate for large-scale MLA fabrication. The sample can be precisely moved by a  $xyz$  piezoelectric stage 200  $\mu\text{m}$   $\times$  200  $\mu\text{m}$   $\times$  200  $\mu\text{m}$  with 1 nm resolution. The optimal rotation angle (ORA) method [21] is used to generate the phase hologram, which has a high iteration speed for few spots.

In order to eliminate the unmodulated zero-order light generated by the pixelation effect, a spherical phase was added to the original hologram to focus it 10  $\mu\text{m}$  above the silica surface. Figure 1(b) shows three types of phase holograms 1080  $\times$  1080 resolution generated by the ORA method with three, four, and five focal spots, respectively, along the optical axis. Flexibility of the holographic algorithm allows for multi-focal spots designed with a 3  $\mu\text{m}$  gap in air between two neighboring spots. The distance ( $\sim 4.6$   $\mu\text{m}$ ) between two spots in silica can be estimated using  $n \times d$ , where  $n$  is the refractive index of the silica, and  $d$  is the distance between two spots in air [22]. The intensity distribution of the holograms at the focus is simulated using a 3D vectorial diffraction theory [23] and illustrated in Fig. 1(c). Multi-spots distributed uniformly along the beam propagation direction with 3  $\mu\text{m}$  interspace agree well with the original design. The first focus is placed on the interface of air and silica (0  $\mu\text{m}$ ), while other foci are inside silica sample [Fig. 1(c)].

Irradiation of the silica sample by fs-laser pulses can cause either of two effects based on laser intensity: ablation and modification. When the pulse intensity is slightly lower than the damage threshold of the silica ( $\sim 2$  J/cm<sup>2</sup>/pulse), the volume at the focus is locally modified due to the alteration of the silica ring structure from five to three members of the Si-O-Si segments [24]. This causes a bond angle change, which in turn leads to the changing of the silica density and refractive index. Densification and formation of three-membered ring structures in silica increases its etch rate in hydrofluoric acid (HF) solution via the Lewis-based mechanism [25], when the angle of the Si-O-Si segment becomes smaller and exposes unpaired electrons of oxygen. This makes silica more chemically reactive with acid—hence, a stronger base.

As the intensity reaches the damage threshold, there is a sub-micrometer-sized ablation crater on the surface of the silica at the center of the irradiation area surrounding the modification

area. Four different single pulse energies—358 nJ, 453 nJ, 545 nJ, and 642 nJ—above the damage threshold were used to investigate the relationship between pulse energy and size of the microlens by one spot irradiation. After the irradiation by a laser pulse, the sample was immersed in HF solution (20% vol.) at 25°C for 40 min etching. A laser confocal microscopy (LSCM, LEXT OLS 4100, Olympus) was used to measure the morphology of the concave microlens.

As shown in Fig. 2(a), all the usual uneven features of the ablation crater disappeared after etching, and the circumference of the lens evolved into a perfect circle for each pulse energy [26]. The cross section of each microlens showed that they all had a spherical profile [Fig. 2(b)]. The size of the microlens depends mainly on the initially modified structure, which was controlled by the pulse energy for the same etching time (40 min). The radius could be tuned from  $\sim 16$   $\mu\text{m}$  to  $\sim 19$   $\mu\text{m}$  when the intensity increased from 358 nJ to 642 nJ [Fig. 2(c)]. The depth changed from  $\sim 3.5$   $\mu\text{m}$  to  $\sim 5.2$   $\mu\text{m}$ , which means a larger volume was modified by the laser pulse near the focus. However, the focal length of all the microlenses remained constant— independent of the energy used for laser inscription. Although the size of the microlens can be slightly controlled by pulse energy, the increments of radius and depth are just about 120% and 150%, respectively, for a  $\sim 180\%$  pulse energy increase. A weak correlation between the pulse energy and microlens size, which rely mainly on the modification depth at the irradiated volume, limits the processing flexibility of this method and makes inefficient usage of the laser pulse energy.

In order to increase the efficiency of the pulse energy for microlens fabrication and to control its size, we propose a simple and effective method to regulate the depth of the laser-modified region in silica by using a SLM. As shown in Fig. 2, there is a correlation between microlens size and the modification depth, but it has to be enhanced. The fs-laser beam was split into several spots along the optical axis with a 3  $\mu\text{m}$  interspace, just as illustrated in Fig. 1(c). By keeping the pulse energy constant at 645 nJ, and structuring the intensity along pulse propagation, it is possible to fabricate microlenses by a single pulse writing/exposure. After etching in 20% HF solution for 40 min, the morphology of the microlenses was

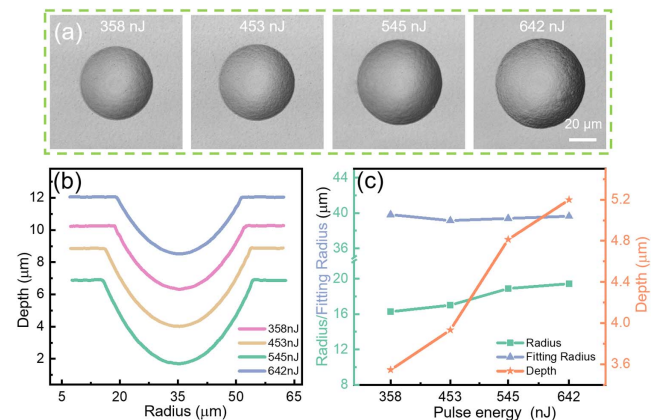


**Fig. 2.** Microlens defined by a single spot irradiation. (a) Top view of the microlens after etching for 40 min in 20% HF solution initially irradiates different pulse energies: 358 nJ, 453 nJ, 545 nJ, 642 nJ. (b) Profile of the microlens corresponding to the different pulse energies. (c) Radius, depth, and fitting radius (the curvature radius) of the microlens.

measured as shown in Figs. 3(a)–3(b). The top view shows that all the microlenses have a circular outline, which means that all of the laser-modified area has been removed (ablation spot is irregular). The R-square value is 0.997 when a circle's equation is used for fitting the cross section, which demonstrates that the microlens has a spherical surface. The final diameter of the microlens is dependent on the depth of the laser-modified region due to the isotropic etching of silica in HF solution, while the modified region is etched out by an anisotropic etching. The modification depth is limited by the laser modification depth. When a large number of axial focal spots are used for silica modification, the final depth is larger. In brief, not only the radius but also the depth of microlenses increases with the axially extended modification depth following the increase in the number of focal spots [Fig. 3(b)]. The quantitative analysis results [Fig. 3(c)] show that the radius can be tuned from  $\sim 19 \mu\text{m}$  to  $\sim 34 \mu\text{m}$  just by changing the holograms. The depth can even reach  $\sim 20 \mu\text{m}$  using the six-foci hologram from  $\sim 5 \mu\text{m}$ . The dynamic range of depth control has increased by 400% for the same pulse energy.

The following relations based on geometry and theory are used to estimate the optical parameters of microlenses, including the fitting radius  $R$  (curvature radius), focal length  $f$ , f-number  $f_{\#}$  (capability of collecting light), and the NA [10]:

$$R = (b^2 + r^2)/2b, \quad (1)$$

$$f = R/(n - 1), \quad (2)$$

$$f_{\#} = f/2r, \quad (3)$$

$$\text{NA} = r/f, \quad (4)$$

where  $r$  is the radius of the concave microlens, and  $n$  is the refractive index of silica ( $n = 1.46$ ).

In our experiment, the fitting curvature radius and focal length of microlenses remained almost constant:  $\sim 39.5 \mu\text{m}$  for radius and  $\sim 86 \mu\text{m}$  for focal length, with a small deviation of 3.9% [Fig. 3(d)]. The NA of the microlenses calculated by the

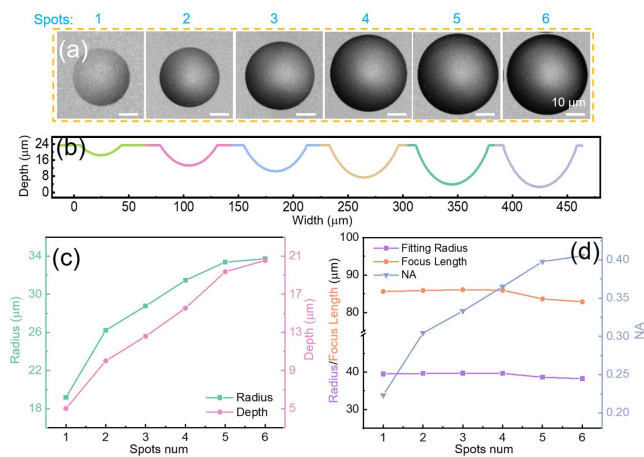


**Fig. 3.** Microlens defined by a multi-focus irradiation. (a) Top view of the microlens after etching for 40 min in 20% HF solution with different numbers of foci along the optical axis from one to six. (b) Profile of the microlens corresponding to the different numbers of foci. (c) Radius, depth of the microlens etched after irradiation by a different number of foci. (d) Relationship between number of foci and the focal length and NA of the microlenses.

above equation exhibited an approximately linear relationship with the number of foci, which ranged from 0.22 at one spot to 0.41 at six spots. The lower NA increment from five to six spots was caused mainly by the lower energy at each spot with the total energy invariant. A high-NA microlens could be obtained by higher pulse energy.

Finally, we used the dynamic single-pulse holographic fs-laser processing system to fabricate a MLA with different microlens sizes just by changing the holograms and keeping the energy constant at 645 nJ. A large area of  $1.5 \text{ mm} \times 1.5 \text{ mm}$  with different sizes and  $65 \mu\text{m}$  interspace MLA was realized in 10 min with a low laser frequency of 1 Hz. The processing efficiency was considerably augmented, since the frequency of SLM refresh was 60 Hz. The top view and the 3D profiles of the MLA are shown in Fig. 4(b), respectively. The sizes are uniform and shapes are consistent with our measurements for every microlens. The imaging ability of the MLA was demonstrated using a microscope [Fig. 4(a)]. Due to the higher light collecting capability, the normalized intensity at focus increased by  $\sim 20\%$  for the first five microlenses, which scaled up with diameter and NA from 0.22 to 0.4 [Fig. 4(c)]. Then it saturated at the last two microlenses due to saturation of NA and chromatic dispersion at focus for a high-NA microlens.

Due to the same top surface and different depths of lenses, the focus of the array with different NA is arranged in 3D space. When using a lower magnification objective ( $10\times$ ) with a large depth of field, the imaging performance of the MLA is captured simultaneously at the same image plane, which means the different reduction of the letter “F” for different microlenses. In order to demonstrate the 3D varying focusing performance, the imaging performance was measured at different image planes. As shown in Fig. 4(c)(iii), when the last lens shows a clear image, the rest of the microlenses have larger but blurred images (especially the second one). In addition, the size of the image-F gradually increases with the reducing NA and increasing defocusing distance. To avoid the defocusing of the high NA microlens (small depth of field), we found the best view as shown in Fig. 4(c)(iv), where all the microlenses show a clear image-F. The out-of-focus effect is more obvious for the high-NA microlens when the first one has a clear image [Fig. 4(c)(v)].

Fs-laser modifications in silica glass introduce the anisotropy of wet etching [27], which can also be combined with the intrinsic anisotropy of etching in quartz (crystalline silica) [28] for micro-fluidic application. Etch rate and final surface

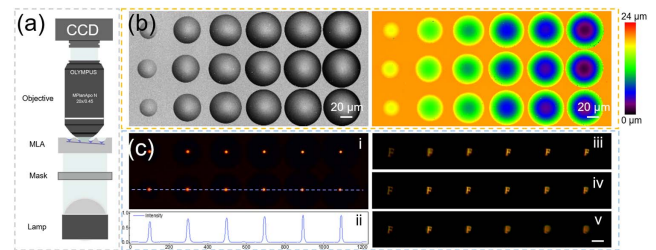


**Fig. 4.** Results of microlens array with different sizes. (a) Schematic diagram of the imaging system for characteristics of microlens arrays. (b) Images measured by laser confocal microscope. (Left: optical image of the MLA. Right: contour map of the MLA.) (c) (i) Focusing characteristic of MLA. (ii) Normalized intensity distribution of the focal spots marked in (i). (iii–v) Imaging performance of MLA at different focusing positions.

quality were dependent on HF concentration [25] as well as the pH value for multi-component glasses. Slower buffered-HF etchants showed a smoother surface [25]. The anisotropy induced by multi-foci modification introduced a strong axial etching anisotropy during the first minutes of etching. Later, a spherical surface was formed and saturated after 35–40 min etching. Longer etching did not make the lenses deeper, for the original surface was receding too. Interestingly, the polarization had no effect for the formation of large-diameter lenses, as we see in Fig. 4. However, at the very beginning of etching, we saw that nanogratings were affecting the morphology and were material dependent [29].

The proposed method is applicable to other transparent materials as well. It depends mainly on the property of materials rather than the wavelength of the fs laser. For example, sapphire can be etched by HF [30] as well as potassium hydroxide (KOH) [31] while the anisotropy is laser inscribed. In crystals, the amorphous phase is induced by fs-laser pulses and can be utilized for removal by wet etching [30]. The presented method to etch optical elements following the inscribed patterns and guiding the anisotropy of etching can find wide applications in the fabrication of 3D complex structures on different glasses and crystals [25,32–35]. We expect that the demonstrated method would also work with different axial intensity patterns [27,36–39].

In summary, we proposed a single-pulse light-shaping method for the fabrication of controllable microlenses inside silica. The relationship between the spots number in the multi-foci array and the diameter of the microlens was established. By keeping the same pulse energy and etching time, the radius and the depth of a single microlens increased 200% and 400% compared with a single focus irradiation, respectively. Finally, the fabrication of a series of variable sized MLAs was demonstrated by a simple dynamic holographic processing. The fabricated MLAs had good light collection capability and imaging performance with a dynamic range of NAs from 0.2 to 0.4. This novel spot-shaping method greatly enhanced the efficiency and flexibility of fs-laser dynamic holographic processing. It provides an effective approach for the manufacturing/fabrication of MLAs of different sizes and NAs, which have significant potential in the areas of microfluidic chips, beam shaping, microsensors, and zoom-less imaging systems.

**Funding.** Australian Research Council (Discovery DP190103284 grant); National Key Research and Development Program of China (2017YFB1104600); National Science Foundation of China (61435005, 61590930, 61825502, 61827826).

**Acknowledgment.** S. J. is grateful for support via the Changjiang Distinguished Professor project on 3D laser nano/micro-printing at Jilin University and to Vijay Kumar for critical reading of the paper. S. J. acknowledges support via the ARC Discovery grant. The authors acknowledge support by the National Key Research and Development Program of China and National Natural Science Foundation of China (NSFC).

## REFERENCES

1. Y. Wu, M. K. Sharma, and A. Veeraraghavan, *Light Sci. Appl.* **8**, 44 (2019).
2. S. Matsuo, T. Miyamoto, T. Tomita, and S. Hashimoto, *Appl. Opt.* **46**, 8264 (2007).
3. J.-Y. Hu, C.-P. Lin, S.-Y. Hung, H. Yang, and C.-K. Chao, *Sens. Actuators A Phys.* **147**, 93 (2008).
4. V. Lin, H.-C. Wei, H.-T. Hsieh, J.-L. Hsieh, and G.-D. Su, *Micro Nano Lett.* **6**, 523 (2011).
5. E. Schonbrun, P. E. Steinvurzel, and K. B. Crozier, *Opt. Express* **19**, 1385 (2011).
6. S.-H. Eom, E. Wrzesniewski, and J. Xue, *Org. Electron.* **12**, 472 (2011).
7. N. Ong, Y. Koh, and Y. Q. Fu, *Microelectron. Eng.* **60**, 365 (2002).
8. J.-J. Yang, Y.-S. Liao, and C.-F. Chen, *Opt. Commun.* **270**, 433 (2007).
9. E. Roy, B. Voisin, J.-F. Gravel, R. Peytavi, D. Boudreau, and T. Veres, *Microelectron. Eng.* **86**, 2255 (2009).
10. R. Ahmed, A. K. Yetisen, and H. Butt, *ACS Nano* **11**, 3155 (2017).
11. Y. Bellouard, A. Said, M. Dugan, and P. Bado, *Opt. Express* **12**, 2120 (2004).
12. R. Osellame, H. Hoekstra, G. Cerullo, and M. Pollnau, *Laser Photon. Rev.* **5**, 442 (2011).
13. Z.-C. Ma, X.-Y. Hu, Y.-L. Zhang, X.-Q. Liu, Z.-S. Hou, L.-G. Niu, L. Zhu, B. Han, Q.-D. Chen, and H.-B. Sun, *Adv. Funct. Mater.* **29**, 1903340 (2019).
14. X.-Q. Liu, Q.-D. Chen, K.-M. Guan, Z.-C. Ma, Y.-H. Yu, Q.-K. Li, Z.-N. Tian, and H.-B. Sun, *Laser Photon. Rev.* **11**, 1600115 (2017).
15. Z. Deng, F. Chen, Q. Yang, H. Bian, G. Du, J. Yong, C. Shan, and X. Hou, *Adv. Funct. Mater.* **26**, 1995 (2016).
16. F. Chen, H. Liu, Q. Yang, X. Wang, C. Hou, H. Bian, W. Liang, J. Si, and X. Hou, *Opt. Express* **18**, 20334 (2010).
17. Z. Deng, Q. Yang, F. Chen, X. Meng, H. Bian, J. Yong, C. Shan, and X. Hou, *Opt. Lett.* **40**, 1928 (2015).
18. C. Xin, L. Yang, J. Li, Y. Hu, D. Qian, S. Fan, K. Hu, Z. Cai, H. Wu, D. Wang, and D. Wu, *Adv. Mater.* **31**, 1808226 (2019).
19. J. Ni, C. Wang, C. Zhang, Y. Hu, L. Yang, Z. Lao, B. Xu, J. Li, D. Wu, and J. Chu, *Light Sci. Appl.* **6**, e17011 (2017).
20. C. Wang, L. Yang, Y. Hu, S. Rao, Y. Wang, D. Pan, S. Ji, C. Zhang, Y. Su, W. Zhu, and J. Li, *ACS Nano* **13**, 4667 (2019).
21. B. Sun, P. S. Salter, C. Roeder, A. Jesacher, J. Strauss, J. Heberle, M. Schmidt, and M. J. Booth, *Light Sci. Appl.* **7**, 17117 (2018).
22. Q. Sun, H. Jiang, Y. Liu, Y. Zhou, H. Yang, and Q. Gong, *J. Opt. A* **7**, 655 (2005).
23. S. Ji, L. Yang, C. Zhang, Z. Cai, Y. Hu, J. Li, D. Wu, and J. Chu, *Opt. Lett.* **43**, 3514 (2018).
24. R. Stoian, M. Bhuyan, A. Rudenko, J.-P. Colombier, and G. Cheng, *Adv. Phys. X* **4**, 1659180 (2019).
25. S. Juodkazis, K. Yamasaki, V. Mizeikis, S. Matsuo, and H. Misawa, *Appl. Phys. A* **79**, 1549 (2004).
26. X.-W. Cao, Q.-D. Chen, L. Zhang, Z.-N. Tian, Q.-K. Li, L. Wang, S. Juodkazis, and H.-B. Sun, *Opt. Lett.* **43**, 831 (2018).
27. A. Marcinkevicius, S. Juodkazis, S. Matsuo, V. Mizeikis, and H. Misawa, *Jpn. J. Appl. Phys.* **40**, L1197 (2001).
28. S. Matsuo, Y. Tabuchi, T. Okada, S. Juodkazis, and H. Misawa, *Appl. Phys. A* **84**, 99 (2006).
29. X.-W. Cao, Q.-D. Chen, H. Fan, L. Zhang, S. Juodkazis, and H.-B. Sun, *Nanomaterials* **8**, 287 (2018).
30. S. Juodkazis, K. Nishimura, S. Tanaka, H. Misawa, E. E. Gamaly, B. Luther-Davies, L. Hallo, P. Nicolai, and V. Tikhonchuk, *Phys. Rev. Lett.* **96**, 166101 (2006).
31. S. Juodkazis, Y. Nishi, and H. Misawa, *Phys. Stat. Solidi* **2**, 275 (2008).
32. A. Ródenas, M. Gu, G. Corrielli, P. Paiè, S. John, A. K. Kar, and R. Osellame, *Nat. Photonics* **13**, 105 (2019).
33. M. Beresna, M. Gecevicius, P. Kazansky, and T. Gertus, *Appl. Phys. Lett.* **98**, 201101 (2011).
34. P. Kazansky, H. Inouye, T. Mitsuyu, K. Miura, J. Qiu, K. Hirao, and F. Starrost, *Phys. Rev. Lett.* **82**, 2199 (1999).
35. S. Juodkazis, S. Matsuo, H. Misawa, V. Mizeikis, A. Marcinkevicius, H.-B. Sun, Y. Tokuda, M. Takahashi, T. Yoko, and J. Nishii, *Appl. Surf. Sci.* **197**, 705 (2001).
36. M. K. Bhuyan, F. Courvoisier, P. A. Lacourt, M. Jacquot, R. Salut, L. Furfaro, and J. M. Dudley, *Appl. Phys. Lett.* **97**, 081102 (2010).
37. G. Wang, Y. Yu, L. Jiang, X. Li, Q. Xie, and Y. Lu, *Appl. Phys. Lett.* **110**, 161907 (2017).
38. M. Duocastella and C. B. Arnold, *Laser Photon. Rev.* **6**, 607 (2012).
39. L. Wang, Q.-D. Chen, X.-W. Cao, R. Buividas, X. Wang, S. Juodkazis, and H.-B. Sun, *Light Sci. Appl.* **6**, e17112 (2017).